

Tsampras, Georgios, Richard Sause, "Force-Based Design Method for Force-Limiting Deformable Connections in Earthquake-Resistant Buildings." *Journal of Structural Engineering*, 10.1061/(ASCE)ST.1943-541X.0003456

# Force-based design method for force-limiting deformable connections in earthquake-resistant buildings

Georgios Tsampras, Ph.D., M.ASCE<sup>1</sup> and Richard Sause, Ph.D., P.E., M.ASCE<sup>2</sup>

<sup>1</sup>Assistant Professor of Structural Engineering, UC San Diego, 9500 Gilman Drive, La Jolla, CA  
92093, gtsampras@ucsd.edu

<sup>2</sup>Joseph T. Stuart Professor of Structural Engineering, Lehigh University, 117  
ATLSS/Mountaintop Drive, Bethlehem, PA 18015, rs0c@lehigh.edu

## ABSTRACT

This paper proposes a force-based design method for force-limiting deformable connections that are used to transfer seismic-induced horizontal forces from the floor-diaphragms in buildings to the vertical elements of lateral seismic force-resisting systems with base flexural mechanisms (e.g., reinforced concrete shear walls). The design method determines the limiting forces for the connections at each floor of the building. The limiting forces for the connections are the forces at which the force-limiting deformable connections transition from linear-elastic to post-elastic response. The proposed design method is a modified version of the ASCE/SEI 7-16 alternative seismic design force method for floor-diaphragms. Design examples are presented. Seismic responses from numerical simulations of twelve-story, eight-story, and four-story reinforced concrete shear wall example buildings show that the proposed method enables effective preliminary design of the force-limiting deformable connections. It is shown that the buildings with connections designed with the proposed method have relatively uniform distribution of connection deformation demands over the building height. It is also shown that their seismic force and acceleration responses

22 have reduced magnitude and reduced variability compared to conventional buildings that exhibit  
23 large variability in their acceleration responses.

## 24 **Introduction**

25 The design of conventional earthquake-resistant building systems is associated with uncertainty  
26 in the prediction of their seismic response. This uncertainty is a result of the variability in the  
27 earthquake ground motions, and the variability in the structural characteristics and their evolution  
28 during seismic response, which in turn affects the nonlinear response of the building components  
29 (FEMA 2017; Sattar et al. 2018). More specifically, the variability in the seismic response of  
30 structural connections can be high due to the complex interactions resulting from the kinematic  
31 compatibility between structural components. For example, the interaction between the floor-  
32 diaphragms in the gravity load resisting system (GLRS) and the reinforced concrete shear wall  
33 lateral seismic force-resisting systems (LFRS) may lead to damage of the connection (Moehle  
34 et al. 2010) that results in uncontrolled transfer of forces. Because of the uncontrolled response,  
35 the seismic-induced horizontal forces in the floor-diaphragms can be large relative to the floor-  
36 diaphragm strength, and may lead to non-ductile response of the diaphragms (Fleischman and  
37 Farrow 2001). The development of excessive inertia forces due to high floor accelerations can  
38 produce nonlinear response and significant damage of the LFRS (Rodriguez et al. 2002). In  
39 addition, the peak floor accelerations can be much larger than the peak ground accelerations,  
40 when both the 1st and higher modes are fully considered in the dynamic response of buildings  
41 (Ray-Chaudhuri and Hutchinson 2011).

### 42 **Review of force-limiting deformable connections in earthquake-resisting buildings**

43 Crane 2004 conducted shake table tests on two small-scale six-story buildings with energy  
44 dissipative connections between the floors and the LFRS. Triangular-plate added damping and  
45 stiffness devices were used as the connections. Reduced floor accelerations and base overturning  
46 moment were observed.

47 Zhang et al. 2014 and Fleischman et al. 2015 introduced an innovative inertia force-limiting  
48 system for earthquake-resistant buildings. The innovative system uses force-limiting deformable  
49 connections between the floor-diaphragms of a flexible GLRS and the stiff vertically-oriented  
50 LFRS of an earthquake-resistant building. Fig. 1 shows a schematic example of a reinforced  
51 concrete shear wall earthquake-resistant building with force-limiting deformable connections that  
52 consist of a friction device and rubber bearings. Floor openings are introduced around the planar  
53 shear walls. The force-limiting deformable connections allow relative displacement between the  
54 floor-diaphragms and the LFRS, and transfer the seismic-induced horizontal forces from the floor-  
55 diaphragms to the LFRS. The compressive stiffness of the rubber bearings ensures the out-of-plane  
56 stability of the shear walls. The shear stiffness of the rubber bearings provides post-elastic stiffness  
57 to the deformable connections required to limit the inelastic deformation demands between the floors  
58 and the shear wall LFRS. Any vertical motion of the shear wall at each floor level is constrained  
59 only by the shear stiffness of the rubber bearings.

60 Tsampras et al. 2016 presented the development of the force-limiting deformable connection,  
61 where the objectives were to limit the seismic-induced horizontal forces transferred from the floor-  
62 diaphragms in buildings to the vertical elements of LFRS which have a base flexural mechanism  
63 (e.g., reinforced concrete shear walls) and to reduce the seismic-induced horizontal floor acceler-  
64 ations of these buildings. More specifically, the authors performed a parametric numerical study  
65 of an example twelve-story building model with force-limiting deformable connections that have  
66 idealized bilinear elastic-plastic connection force-deformation responses. The parametric study  
67 defined an approximate feasible design space for the following three properties of the force-limiting  
68 deformable connections: (1) their limiting force (i.e., the force at which each deformable con-  
69 nection at each floor transitions from linear-elastic to post-elastic response), (2) their linear-elastic  
70 stiffness, and (3) their post-elastic stiffness. The parametric study assumed that the force-limiting  
71 deformable connections have the same (i.e., constant) properties over the height of the building.  
72 It was concluded that a force-limiting deformable connection consisting of a friction device or a  
73 buckling-restrained brace with low damping rubber bearings can provide a combination of limiting

74 force, linear-elastic stiffness, and post-elastic stiffness that is within the approximate feasible design  
75 space.

76 Tsampras and Sause 2014a, Tsampras and Sause 2014b, Tsampras et al. 2017, and Tsampras et al.  
77 2018 presented detailed experimental studies of full-scale force-limiting deformable connections  
78 conducted at the experimental facility NHERI at Lehigh (Cao et al. 2020). Fleischman et al.  
79 2014 and Zhang et al. 2018 discussed the shake-table experimental seismic response of a half-  
80 scale, four-story reinforced concrete flat-plate shear wall structure with force-limiting deformable  
81 connections subjected to a sequence of twenty-two ground motions simulated at the experimental  
82 facility NHERI at UC San Diego (Van Den Einde et al. 2021).

83 Tsampras et al. 2016 conducted numerical earthquake simulations to compare the seismic  
84 response of an example twelve-story reinforced concrete shear wall building model with exper-  
85 imentally calibrated force-limiting deformable connection models with the seismic response of  
86 the example building model with monolithic "rigid" (RE) connections. The RE connections  
87 had high linear-elastic stiffness compared to the stiffness of the connecting structural compo-  
88 nents and unbounded (infinite) strength. The RE connections simulated the connections between  
89 floor-diaphragms and LFRS in a conventional building. The value of the limiting force of each  
90 deformable connection at each floor of the building was the same (i.e., the connections had constant  
91 limiting force values over the height of the building) and equal to a value within the approximate  
92 feasible design space estimated in the parametric study discussed earlier. The authors concluded  
93 that the use of force-limiting deformable connections resolves the issues associated with complex  
94 interactions from kinematic compatibilities between the floor-diaphragms and the LFRS that may  
95 be difficult to accommodate with "rigid" monolithic connections. In addition, it was observed that  
96 the use of force-limiting deformable connections: (1) limits the story shear forces, floor acceler-  
97 ations, base shear, and forces transferred from the floor-diaphragms to the LFRS, (2) reduces the  
98 variability in the story shear forces, floor accelerations, base shear, and forces transferred from the  
99 floor-diaphragms to the LFRS due to the ground motion variability, and (3) mitigates the effects of  
100 higher mode responses on the dynamic response of the building.

101 The past research studies, however, also showed that the connection deformation demands de-  
102 pend on the numerical model of the GLRS. More specifically, Tsampras 2016 conducted numerical  
103 earthquake simulations to assess the effect of the GLRS model on the seismic response of an exam-  
104 ple twelve-story building with force-limiting deformable connections with constant limiting force  
105 over the height of the building. The results from the numerical earthquake simulations showed that  
106 reducing the stiffness of the GLRS model increases the GLRS story drift demands and the con-  
107 nection deformation demands without significantly affecting the LFRS story shears, GLRS story  
108 shears, connection forces, LFRS story drifts, and floor total accelerations. The building model with  
109 a pin-base lean-on column GLRS model resulted in the largest connection deformation demands.  
110 The connection deformation demands were larger at the top floors compared to the demands at the  
111 lower floors (i.e., the connection deformations were non-uniform over the height of the building).

112 Considering the findings from the past research studies discussed above, it is concluded that  
113 there is the need for a simple and efficient method to determine the design value of the limiting  
114 force for each deformable connection at each floor of a building. A building with force-limiting  
115 deformable connections designed using this method should have reasonable magnitudes and a  
116 relatively uniform distribution of connection deformation demands over the building height, even  
117 when a flexible pin-base lean-on column GLRS model is assumed. These buildings should have  
118 floor accelerations and seismic force responses with reduced magnitude and reduced dispersion  
119 compared to conventional buildings.

## 120 **Scope of study**

121 This paper presents: (1) a force-based design method to determine the design value of the  
122 limiting force for the force-limiting deformable connection at each floor of buildings with LFRS  
123 that have a base flexural mechanism (e.g., reinforced concrete shear wall buildings), (2) design  
124 examples, and (3) numerical simulations of twelve-story, eight-story, and four-story reinforced  
125 concrete shear wall example buildings with force-limiting deformable connections designed using  
126 the proposed method. The proposed design method is a modified version of the ASCE/SEI 7-  
127 16 (ASCE 2017) alternative seismic design force method for floor-diaphragms. The method is

128 simple to implement in design practice. The method is also efficient since it does not require a  
129 large number of parametric numerical earthquake simulations to determine a feasible design space  
130 for the design values of the limiting force. The method provides design values for the limiting  
131 force that vary appropriately over the height of the building (e.g., larger limiting forces at the  
132 top floors compared to the lower floors of a building) by considering the relative contributions of  
133 the first and higher modes to the seismic response of the building. The design examples show  
134 design values for the limiting forces of force-limiting deformable connections for twelve-story,  
135 eight-story, and four-story reinforced concrete shear wall example buildings. Seismic responses  
136 from numerical earthquake simulations of these example buildings with force-limiting deformable  
137 connections designed using the proposed design method are compared with the seismic responses of  
138 the example buildings with deformable connections with a constant limiting force over the height  
139 of the building, and with the seismic responses of the example buildings with RE connections,  
140 which represent conventional buildings. The effect of the number of stories in the building and the  
141 magnitude of the limiting forces of the connections on the seismic response of the example buildings  
142 is studied. It is shown that the buildings with force-limiting deformable connections designed using  
143 the proposed method have a more uniform distribution of connection deformation demands over  
144 the height of the building compared to the buildings with deformable connections with constant  
145 limiting force values over the height of the building. Larger design values of the limiting force are  
146 required in the four-story building to have connection deformation demands similar to those of the  
147 eight-story and the twelve-story buildings. It is also shown that the buildings with force-limiting  
148 deformable connections designed using the proposed method have floor accelerations and force  
149 responses with reduced magnitude and dispersion compared to buildings with RE connections.  
150 The reduced magnitude and dispersion of the floor acceleration response reduces the potential  
151 for damage to acceleration sensitive nonstructural components, and reduces the uncertainty in the  
152 seismic response of the structural components of the building.

# Force-based design method for force-limiting deformable connections

## Review of alternative seismic design force for floor-diaphragms

As an introduction to the proposed design method, this section summarizes the calculation of the alternative seismic design force for floor-diaphragms at elevation level  $x$  denoted as  $F_{px}$  [Eq. 1], presented in FEMA P-1050 (FEMA 2015). This method was adapted by ASCE/SEI 7-16 with modifications.

$$F_{px} = \frac{C_{px}}{R_s} w_{px} \geq 0.2 S_{DS} I_e w_{px} \quad (1)$$

where  $C_{px}$  is the design acceleration coefficient at level  $x$ ,  $R_s$  is the diaphragm design force reduction factor,  $w_{px}$  is the seismic weight tributary to the diaphragm at level  $x$ ,  $S_{DS}$  is the design spectral acceleration at short periods, and  $I_e$  is the importance factor. The possible distributions of values of  $C_{px}$  based on the total number of floors  $n$ , are shown in Fig. 2 (FEMA 2015). The amplification of  $C_{px}$  at  $h_x/h_n \geq 0.8$  for  $n \geq 3$  is related to the second and higher mode contributions to the total force response. The design acceleration coefficients  $C_{p0}$  at the base and  $C_{pn}$  at the top level  $n$  are defined below:

$$C_{p0} = 0.4 S_{DS} I_e \quad (2)$$

$$C_{pn} = \sqrt{(\Gamma_{m1} \Omega_0 C_s)^2 + (\Gamma_{m2} C_{s2})^2} \quad (3)$$

$$\Gamma_{m1} = 1 + \frac{z_s}{2} \left(1 - \frac{1}{n}\right) \quad (4)$$

$$\Gamma_{m2} = 0.9 z_s \left(1 - \frac{1}{n}\right)^2 \quad (5)$$

$$C_{s2} = \begin{cases} \min \left[ \frac{I_e S_{D1}}{0.03(n-1)}; (0.15n + 0.25) I_e S_{DS}; I_e S_{DS} \right], & \text{for } n \geq 2 \\ 0, & \text{for } n = 1 \end{cases} \quad (6)$$

where  $\Gamma_{m1}$  is the first mode contribution factor,  $\Omega_0$  is the LFRS overstrength factor,  $C_s$  is the seismic response coefficient,  $\Gamma_{m2}$  is the higher mode contribution factor (assuming one contribution factor

for all the modes higher than the first mode),  $C_{s2}$  is the higher mode seismic response coefficient, and  $z_s$  is the mode shape factor equal to 0.30 for buckling restrained braced frames, 0.70 for moment resisting frames, 0.85 for dual systems, and 1.00 for all other systems.

### Seismic load path

This section reviews the path of seismic-induced horizontal forces in buildings with force-limiting deformable connections between the GLRS and LFRS of a building. Fig. 3 shows the seismic-induced forces acting in the GLRS and LFRS in the undeformed position of the building. For the GLRS, which is assumed to contain the majority of the seismic mass, the inertia forces due to the total acceleration are denoted  $F_{I,GLRS}$ , the viscous damping forces are denoted  $F_D$ , the restoring forces due to the frame action and overturning resistance of the GLRS are denoted  $F_{S,GLRS}$ . The forces transferred from the GLRS to the LFRS through the force-limiting deformable connections are denoted  $F_{DC}$ . For the LFRS the inertia forces due to the total acceleration are denoted  $F_{I,LFRS}$ , the restoring forces for the LFRS (i.e., shear wall) are denoted  $F_{S,LFRS}$ . For clarity, the forces in the rubber bearings and the forces developed due to the out-of-plane action of the walls are not shown in Fig. 3.

The restoring forces  $F_{S,GLRS}$  and damping forces  $F_D$  of the GLRS are not zero. However, for preliminary design purposes, we assume that the seismic-induced horizontal forces are resisted entirely by the vertical elements of the LFRS, the force-limiting deformable connections, and the diaphragm. Therefore, for preliminary design, the restoring forces  $F_{S,GLRS}$  and damping forces  $F_D$  of the GLRS are assumed to be negligible and  $F_{I,GLRS}$  are in equilibrium with  $F_{DC}$ . In addition, if the mass associated with the shear wall is considered negligible (i.e., very small compared to the total seismic mass),  $F_{DC}$  are in equilibrium with  $F_{S,LFRS}$ . Thus, as a simplification for preliminary design, we can determine design values for the limiting force for each deformable connection at each floor of the building from an estimate of the inertia forces in each floor-diaphragm. In the next section the proposed force-based procedure for the design of the force-limiting deformable connections is presented.



## Design values for limiting force for deformable connection at each floor

The calculations of  $F_{px}$  presented earlier, are modified to determine design values for the limiting force for the deformable connection at each floor of the building. The modified calculations are shown in the following equations:

$$F_{Lx} = \frac{C_{Lx} w_{px}}{R_{DC} n_{Lx}} \quad (7)$$

$$C_{L0} = 0.4S_{DS}I_e \quad (8)$$

$$C_{Ln} = \sqrt{(\Gamma_{m1}C_s)^2 + (\Gamma_{m2}C_{s2})^2} \quad (9)$$

where  $F_{Lx}$  is the design limiting force for the deformable connection at level  $x$ , which is the target force value when the connection response transitions from linear-elastic to post-elastic,  $C_{Lx}$  is the design acceleration coefficient at level  $x$ ,  $C_{Ln}$  is the design acceleration coefficient at level  $n$ ,  $C_{L0}$  is design acceleration coefficient at the base of the building, and  $R_{DC}$  is the deformable connection design force factor that accounts for the deformation capacity of the deformable connection. Specific values are not given for  $R_{DC}$  in this section. Possible values of  $R_{DC}$  will be assessed and discussed later.  $w_{px}$  is the seismic weight tributary to the diaphragm at level  $x$ ,  $n_{Lx}$  is the number of force-limiting deformable connections at level  $x$ ,  $S_{DS}$  is the design spectral acceleration at short periods, and  $I_e$  is the importance factor (FEMA 2015).  $C_{Lx}$  and  $F_{Lx}$  for  $n \geq 3$  (assuming  $w_{px}$ ,  $R_{DC}$ , and  $n_{Lx}$  are the same for each floor) are shown in Fig. 4.  $F_{Lx}$  is used to design the force-limiting deformable connections at level  $x$ .

The calculations were modified to seek a balanced distribution of inelastic deformation demand between the force-limiting deformable connections and the flexural yielding base mechanism of the LFRS. The modifications are the following: (1) The participation of the first mode in  $C_{Ln}$  in Equation 9 is not amplified by the LFRS overstrength factor  $\Omega_0$  in comparison to  $C_{pn}$  in Equation 3 since the calculation of  $F_{Lx}$  assumes that no significant hardening has occurred at the base flexural yielding mechanism of the LFRS when the force-deformation responses of the deformable connections transition from linear-elastic to post-elastic. (2) The lower limit is not used for  $F_{Lx}$  in

217 Equation 7 in comparison to  $F_{px}$  from Equation 1. (3) The factor  $R_{DC}$  accounts for the deformation  
 218 capacity (i.e., ductility capacity) of the deformable connections instead of the diaphragm design  
 219 force reduction factor  $R_s$  used in Equation 1. The base moment in the LFRS,  $M_{bFLx}$ , calculated  
 220 assuming the  $F_{Lx}$  act concurrently, should be greater than or equal to  $M_{by}$ , which is the moment  
 221 when nonlinear moment-rotation response initiates at the base flexural yielding mechanism of the  
 222 LFRS.  $M_{bFLx}/M_{by} \geq 1.0$  is intended to prevent excessive deformation demands in the force-  
 223 limiting connections and balance the inelastic deformations between the LFRS and connections.  
 224 An upper limit on  $R_{DC}$  is developed as follows:

$$\begin{aligned}
 1.0 &\leq \frac{M_{bFLx}}{M_{by}} \\
 1.0 &\leq \sum_{x=1}^n \frac{F_{Lx} h_x}{M_{by}} \\
 1.0 &\leq \sum_{x=1}^n \frac{C_{Lx} \frac{w_{px}}{n_{Lx}} h_x}{M_{by}} \\
 R_{DC} &\leq \sum_{x=1}^n \frac{C_{Lx} \frac{w_{px}}{n_{Lx}} h_x}{M_{by}} \tag{10}
 \end{aligned}$$

225 The proposed method enables the preliminary design of the force-limiting deformable connections  
 226 without a large number of parametric numerical earthquake simulations. Nonlinear numerical  
 227 earthquake simulations are needed to determine if the building seismic response is acceptable.

## 228 **Design of force-limiting deformable connections for example build-** 229 **ings**

230 This section presents designs for force-limiting deformable connections for twelve-story, eight-  
 231 story, and four-story reinforced concrete shear wall building models from the method proposed in  
 232 the previous section. Various  $R_{DC}$  values are considered. Later in the paper, the seismic responses  
 233 from numerical simulations of twelve-story, eight-story, and four-story buildings with connections

234 designed using the various  $R_{DC}$  values are compared with the seismic responses of twelve-story,  
235 eight-story, and four-story buildings with deformable connections with a constant limiting force  
236  $F_L$  over the height of the building, and with the seismic responses of twelve-story, eight-story, and  
237 four-story buildings with RE connections, which represent conventional buildings.

### 238 **Reinforced concrete shear wall example buildings**

239 The example buildings are bearing wall systems with special reinforced concrete shear walls  
240 (ASCE 2017). Fig. 5(a) shows the typical floor plan for the twelve-story, eight-story, and four-story  
241 buildings. The floor plan dimensions are 30.5 m x 55.0 m. The ASCE/SEI 7 design spectrum  
242 parameters that were used are  $S_1 = 0.6g$ ,  $S_s = 1.5g$ ,  $F_a = 1.0$ ,  $F_v = 1.5$ ,  $T_{long} = 8.0$  seconds,  
243 Site Class D, and Importance Factor  $I_e = 1.0$  (ASCE 2017). The first story height is 4.9 m and  
244 the remaining story heights are 3.2 m for all three buildings. Symmetry along both plan directions  
245 enabled one half of the building to be modeled and studied. The area tributary to the shear wall and  
246 the gravity system in the model is shown in Fig. 5(a). Each shear wall was assumed to resist half  
247 of the seismic-induced horizontal forces along its plane. The equivalent horizontal seismic force  
248 method was used to design the shear wall of each building (ASCE 2017). The moment at the base  
249 of the shear wall due to the equivalent horizontal seismic forces is denoted  $M_{ELF1}$ .

### 250 **Design values for limiting force for deformable connection at each floor of the example** 251 **buildings**

252 The parameters required to calculate  $C_{Lx}$  for the twelve-story building are parameters for the  
253 design spectrum:  $I_e = 1.0$ ,  $S_{DS} = 1.0$ , and  $S_{D1} = 0.6$ , and parameters for the building:  $z_s = 1.0$ ,  $n$   
254  $= 12$ ,  $C_s = 0.1104$ ,  $C_{s2} = 1.0$ ,  $\Gamma_{m1} = 1.4583$ ,  $\Gamma_{m2} = 0.7563$ ,  $C_{L0} = 0.4$ , and  $C_{Ln} = 0.7732$ . Table  
255 1 lists the quantities required for the calculation of  $F_{Lx}$  used in the deformable connections in the  
256 twelve-story building with  $R_{DC} = 3.0$ . The parameters for the eight-story building are:  $z_s = 1.0$ ,  
257  $n = 8$ ,  $C_s = 0.1473$ ,  $C_{s2} = 1.0$ ,  $\Gamma_{m1} = 1.4375$ ,  $\Gamma_{m2} = 0.6891$ ,  $C_{L0} = 0.4$ , and  $C_{Ln} = 0.7209$ ; and the  
258 parameters for the four-story building are:  $z_s = 1.0$ ,  $n = 4$ ,  $C_s = 0.2$ ,  $C_{s2} = 0.85$ ,  $\Gamma_{m1} = 1.3750$ ,  
259  $\Gamma_{m2} = 0.5063$ ,  $C_{L0} = 0.4$ , and  $C_{Ln} = 0.5107$ . Fig. 6 shows profiles of  $F_{Lx}$  over the height of the  
260 building (i.e., design limiting force values) and the two cases of constant  $F_L$  over the height of the

261 building (denoted as  $F_{L1-1}$  and  $F_{L1-2}$ ), for the twelve-story, eight-story, and four-story buildings.  
 262 For reference, Fig. 6 also includes the one half of the  $F_{px}$  force profile based on ASCE7-10 (ASCE  
 263 2010) and the one half of the  $F_{px}$  force profile based on Eq. (1). The values of  $R_{DC}$  used in the  
 264 design examples satisfy the inequality condition in Eq. (10). For example, for the twelve-story  
 265 building a value of  $R_{DC} = 3.0$  results to  $M_{bFLx}/M_{by} = 1.04 > 1.0$ . Larger values of  $R_{DC}$  would  
 266 result to  $M_{bFLx}/M_{by} < 1.0$ .

## 267 **COMPARISON OF SEISMIC RESPONSES OF BUILDINGS FROM NUMERICAL SIMULATIONS**

### 268 **Reinforced concrete shear wall example building numerical models**

269 Fig. 5(b) shows a schematic of the typical numerical model used for the twelve-story, eight-story,  
 270 and four-story buildings. Linear-elastic beam-column elements were used to model the stiffness of  
 271 the LFRS (shear wall) and GLRS. Nonlinear flexural response and shear failure were not included  
 272 in these elements. For the numerical simulations used to determine the seismic response, nonlinear  
 273 flexural response at the base of the wall, shown in Fig. 5(d), was modeled with a nonlinear spring  
 274 at the base of the wall (described below). Geometric nonlinearities were considered. Table 2 lists  
 275 properties of the linear-elastic beam-column elements used to model the shear wall and properties  
 276 of the base hinge spring used to model the base moment-rotation nonlinear response of the shear  
 277 wall. The wall area  $A_w$ , the wall cracked moment of inertia about the strong axis  $I_{crw}$ , and the  
 278 concrete modulus of elasticity  $E_c$ , are given for the beam-column elements used to model the shear  
 279 wall in each building model.

280 The yield strength and the ultimate capacity of the base hinge spring element,  $M_{by}$ , and  $M_{bcap}$ ,  
 281 respectively, are given in Table 2. The OpenSees (McKenna and Fenves 2021) uniaxial material  
 282 model Pinching4 was used to model the LFRS base hinge nonlinear moment-rotation response  
 283 shown in Fig. 5(d) along with the parameters  $rDispP$ ,  $rForceP$ ,  $uForceP$ ,  $gK1$ ,  $gK2$ ,  $gK3$ ,  
 284  $gK4$ ,  $gKLim$ ,  $gD1$ ,  $gD2$ ,  $gD3$ ,  $gD4$ ,  $gDLim$ ,  $gF1$ ,  $gF2$ ,  $gF3$ ,  $gF4$ ,  $gFLim$ ,  $gE$ , and  $dmgType$   
 285 that are equal to 0.85, 0.85, 0.05, 1.0, 0.0, 0.0, 0.0, 0.995, 0.0, 0.0, 0.0, 0.0, 0.0, 0.0, 0.0,  
 286 0.0, 0.0, 10, and "cycle", respectively. A pin-base lean-on column is used to model the GLRS in  
 287 all buildings, which results in an upper bound of the connection deformation demand (Tsampras

288 2016). Table 3 lists the modulus of elasticity  $E_c$ , the area  $A_c$ , and the moment of inertia  $I_c$  of  
289 the linear-elastic beam-column elements used for the lean-on column in each building model. The  
290 section properties  $A_c$  and  $I_c$  listed in Table 3 are estimated considering the sum of the properties  
291 of the gravity columns within the area tributary to the shear wall.  $I_c$  is estimated considering the  
292 cracked moment of inertia of each gravity column.

293 Fig. 5(c) shows the typical force-limiting deformable connection force-deformation response.  
294 The deformable connections are designed as friction devices and low damping rubber bearings  
295 (Tsampras et al. 2018). All the deformable connections have elastic stiffness  $K_{el} = 1730$  kN/mm  
296 and post-elastic stiffness ratio  $a = 0.005$ .  $F_L$  (Fig. 5(c)) were discussed in previous section and  
297 presented in Fig. 6. The buildings with RE connections have connections that are essentially rigid  
298 and remain linear-elastic, with stiffness equal to 4340 MN/mm.

### 299 Numerical simulations results

300 In this section, results from numerical earthquake simulations of the twelve-story, eight-story,  
301 and four-story buildings with force-limiting deformable connections with  $F_{Lx}$  designed with various  
302  $R_{DC}$  values are compared with the results from numerical earthquake simulations of the twelve-  
303 story, eight-story, and four-story buildings with force-limiting deformable connections with constant  
304  $F_L$  over the height of the building or with RE connections.

305 Eighteen ground motions listed in Table 4 were selected from the FEMA P-695 (FEMA 2009)  
306 far field set and used as input excitation in the numerical earthquake simulations. Each recorded  
307 ground motion was scaled so that the average response spectrum of the scaled ground motions  
308 (Baker 2011) matches the spectral accelerations to the ASCE/SEI 7 (ASCE 2017) design basis  
309 earthquake spectrum over a range of periods  $T \in [0.6, 2.0]$  seconds, as shown in Figure 7. All the  
310 numerical simulations were performed using design basis earthquake level ground motions.

311 Fig. 8 shows seismic responses from numerical simulations for twelve-story buildings. Fig. 9  
312 shows seismic responses from numerical simulations for eight-story and four-story buildings. The  
313 responses plotted in these figures are the floor total acceleration, the force and the deformation in  
314 the connections between the floor-diaphragm of the GLRS and the LFRS, the story shear and the

315 drift of the LFRS, and the story shear and the drift of the GLRS. The peak value of the response  
316 that occurs during each ground motion at each floor or story is shown with a colored marker. The  
317 different colors represent the different cases of the force-limiting deformable connections between  
318 the floors and the LFRS designed with different values for the limiting force; either  $F_{Lx}$  for different  
319  $R_{DC}$  values, or a constant  $F_L$  over the height of the building. The mean value of the peak responses  
320 at each floor or story over the set of ground motions is shown with a white marker for each  
321 connection case. The statistics of the maximum peak floor or story responses of the twelve-story  
322 building shown in Fig. 8 are listed in Table 5, where the "maximum" is the maximum over the  
323 floors or stories of the building, and the statistics are over the ground motions in the set.  $\mu$ ,  $\sigma$ , and  
324  $\sigma/\mu$  denote the mean value, the standard deviation, and the coefficient of variation, respectively.  
325 A discussion on the observations related to each response quantity is presented in the following  
326 paragraphs.

### 327 **Floor total accelerations**

328 The mean peak values of the floor total accelerations and their dispersion is significantly reduced  
329 for the twelve-story buildings with various deformable connection designs compared to those of the  
330 twelve-story building with RE connections. The coefficient of variation of the maximum peak floor  
331 total acceleration in the buildings with force-limiting deformable connections is approximately half  
332 the coefficient of variation of the maximum peak floor total acceleration in the building with RE  
333 connections.

334 The mean peak values of the floor total accelerations and their dispersion for the eight-story  
335 and four-story buildings with deformable connections are smaller than those of the eight-story and  
336 four-story buildings with RE connections. The eight-story and four-story buildings with deformable  
337 connections have similar floor total accelerations.

338 As will be shown later, these observations are attributed to the ability of the force-limiting  
339 deformable connections to mitigate the contribution of the second mode to the total seismic  
340 response.

### Force-limiting deformable connection forces

The mean peak values of the connection forces and their dispersion for the twelve-story buildings with various force-limiting deformable connection designs are significantly reduced compared to those of the twelve-story building with RE connections. The connection forces for the twelve-story buildings with deformable connections are similar, however, the twelve-story building with deformable connections with  $F_{Lx}$  based on  $R_{DC} = 3.0$  has the smallest connection forces. The coefficient of variation for the maximum peak connection force in the buildings with deformable connections is approximately one fifth of the coefficient of variation for the maximum peak connection force in the building with RE connections.

The eight-story and four-story buildings with deformable connections have connection forces that are less than those of the eight-story and four-story buildings with RE connections. The connection forces at the sixth floor of the eight-story buildings with deformable connections are close to the connection force at the sixth floor of the eight-story building with RE connections. The sixth floor of the eight-story building is at 0.77 of the total height of the building which is close to the node of the second mode shape. A similar observation can be made for the third-floor of the four-story building and the tenth-floor of the twelve-story building.

### LFRS (shear wall) story shears

The use of force-limiting deformable connections in the twelve-story buildings reduces the mean peak LFRS story shears and their dispersion compared to the LFRS story shears of the twelve-story building with RE connections. The LFRS story shears in the twelve-story buildings with various deformable connection designs are similar, however, the connections with  $F_{Lx}$  based on  $R_{DC} = 3.0$  result in the smallest mean peak LFRS base (i.e., first story) shear. Note that the mean peak LFRS base shears exceed significantly the design base shear calculated using the ASCE/SEI 7 equivalent lateral force procedure (7835 kN). However, the use of deformable connections reduces the ratio of the mean peak LFRS first story shear over the design base shear. The coefficient of variation for the maximum peak LFRS story shear in the buildings with deformable connections is approximately one quarter of the coefficient of variation for the maximum peak LFRS story shears in the building

368 with RE connections.

369 The eight-story and four-story buildings with various deformable connection designs also have  
370 reduced mean peak LFRS story shears and reduced dispersion of the peak LFRS story shears  
371 compared to those of the eight-story and four-story buildings with RE connections. The eight-story  
372 buildings with deformable connections have similar LFRS story shears, and the four-story buildings  
373 with deformable connections have similar LFRS story shears.

### 374 **Gravity load resisting system (GLRS) story shears**

375 The twelve-story building with RE connections has GLRS story shears in the second and upper  
376 stories with magnitude and dispersion that are less than those of the buildings with force-limiting  
377 deformable connections. As expected, the story shears in the GLRS are significantly less than those  
378 in the LFRS.

379 The eight-story and four-story buildings with various deformable connection designs have  
380 similar GLRS story shears over the height of the building. The magnitude and dispersion of GLRS  
381 story shears in the upper stories are larger than those of the eight-story and four-story buildings with  
382 RE connections. The twelve-story buildings with deformable connections also have GLRS story  
383 shears with magnitude similar to those of the eight-story and four-story buildings with deformable  
384 connections.

### 385 **Force-limiting deformable connection deformations**

386 The twelve-story buildings with force-limiting deformable connections designed for  $F_{Lx}$  that  
387 varies over the height of the building have a more uniform connection deformations over the height  
388 of the building compared to the twelve-story buildings with deformable connections designed for  
389  $F_{L1-1}$  and  $F_{L1-2}$  that do not vary over the height of the building. For  $F_{Lx}$  with a small  $R_{DC}$  value,  
390  $R_{DC} \leq 1.5$ , the connection deformations are nearly constant over the height of the building, and for  
391 a large  $R_{DC}$  value,  $R_{DC} = 3.0$ , the connection deformations increase over the height of the building.  
392 At the twelfth-floor, where the connection deformation is largest, the connection deformation was  
393 smaller with  $F_{Lx}$  based on  $R_{DC} = 3.0$  than for constant  $F_{L1-1}$ , even though  $F_{Lx}$  based  $R_{DC} = 3.0$   
394 does not exceed  $F_{L1-1}$  (for floors 1 through 9,  $F_{Lx}$  with  $R_{DC} = 3.0$  is  $0.50F_{L1-1}$ , and for floors 10,



395 11, and 12,  $F_{Lx}$  with  $R_{DC} = 3.0$  is  $0.59F_{L1-1}$ ,  $0.78F_{L1-1}$ , and  $0.97F_{L1-1}$ , respectively).

396 The eight-story buildings with deformable connections designed for  $F_{Lx}$  have smaller con-  
397 nection deformations at the top two floors compared to the eight-story buildings with deformable  
398 connections designed for  $F_{L1-1}$  and  $F_{L1-2}$ . The four-story buildings with deformable connections  
399 designed for  $F_{Lx}$  based on  $R_{DC} = 1.5$  or  $1.7$  have connection deformations similar to those of the  
400 four-story buildings with deformable connections designed for  $F_{L1-1}$  and  $F_{L1-2}$ . The four-story  
401 buildings with deformable connections designed for  $F_{Lx}$  based on  $R_{DC} \leq 1.2$  have connection  
402 deformations at the top two floors that are smaller than the connection deformations at the top two  
403 floors of the four-story buildings with deformable connections designed for  $F_{L1-1}$  and  $F_{L1-2}$ .

#### 404 **LFRS (shear wall) story drifts**

405 The LFRS story drifts in all buildings are relatively uniform over the height of the building. The  
406 twelve-story buildings with force-limiting deformable connections have smaller LFRS story drifts  
407 than the building with RE connections. The twelve-story building with deformable connections  
408 designed for  $F_{Lx}$  with  $R_{DC} = 3.0$  has the smallest LFRS story drifts.

409 The eight-story and four-story buildings with deformable connections also have smaller LFRS  
410 drifts than the eight-story and four-story buildings with RE connections, respectively.

#### 411 **Gravity load resisting system (GLRS) story drifts**

412 The twelve-story buildings with force-limiting deformable connections designed for  $F_{L1-1}$  and  
413  $F_{L1-2}$  have larger GLRS drifts in the top two stories compared to the building with RE connections.  
414 The twelve-story buildings with deformable connections designed for  $F_{Lx}$  have smaller or similar  
415 GLRS story drifts compared to those of the twelve-story building with RE connections.

416 The GLRS story drifts in the top two stories of the eight-story buildings with deformable  
417 connections designed for  $F_{L1-1}$  and  $F_{L1-2}$  are larger than the GLRS story drift in the top two  
418 stories of the eight-story building with RE connections. The eight-story buildings with deformable  
419 connections designed for  $F_{Lx}$  have GLRS story drifts smaller than or similar to the GLRS story  
420 drifts of the eight-story building with RE connections. The four-story buildings with deformable  
421 connections have larger GLRS story drifts in the top story compared to the four-story building with

RE connections. However, the four-story buildings with deformable connections have GLRS drifts in the remaining stories similar to those of the four-story building with RE connections.

### Effect of $R_{DC}$ and number of stories

This section presents a discussion on the effect of the  $R_{DC}$  value and the number of building stories on the mean of the maximum peak floor or story seismic responses. Each individual plot in Fig. 10 shows the mean of the maximum peak value of a seismic response on the y-axis with respect to the  $R_{DC}$  values on the x-axis. The twelve-story, eight-story, and four-story building results are shown with black circles, red rectangles, and white triangles, respectively. Row 1 of the plots in Fig. 10 shows the mean maximum peak value of seismic responses of buildings with force-limiting deformable connections designed for  $F_{Lx}$  with various  $R_{DC}$  values, denoted  $\mu_{FLx}$ . Row 2 of the plots in Fig. 10 show  $\mu_{FLx}$  normalized by the mean maximum peak value of the seismic response of buildings with force-limiting deformable connections with  $F_{L1-1}$ , denoted  $\mu_{FL1-1}$ . Row 3 of the plots in Fig. 10 shows  $\mu_{FLx}$  normalized by the seismic responses of buildings with RE connections, denoted  $\mu_{RE}$ .

The values of  $\mu_{FLx}$  for the connection deformation depend on the number of stories and the  $R_{DC}$  value. The connection deformation  $\mu_{FLx} \approx 50$  mm and  $\mu_{FLx}/\mu_{FL1-1} \approx 0.5$  in twelve-story, eight-story, and four-story buildings when  $R_{DC}$  equals 2, 1.5, and 0.8, respectively. The connection deformation  $\mu_{FLx}/\mu_{FL1-1} < 1.0$  for every  $R_{DC}$  values and number of stories, while it approaches 1.0 when  $R_{DC} = 1.7$  or 1.5 in the four-story building. Thus, four-story buildings require smaller  $R_{DC}$  values than eight-story and twelve-story buildings to ensure reasonable connection deformations  $\mu_{FLx}$ . The deformation in the RE connections is essentially zero. Thus,  $\mu_{FLx}/\mu_{RE}$  is not defined for the connection deformation response and no plot is not shown in the first column of the third row in Fig. 10.

The floor acceleration and connection force  $\mu_{FLx}$  depend on  $R_{DC}$  but they are essentially independent of the number of stories. The floor acceleration and connection force  $\mu_{FLx}/\mu_{FL1-1} \leq 1.0$  for  $R_{DC} \geq 1.5$ , and  $\mu_{FLx}/\mu_{RE} \leq 0.75$  for every  $R_{DC}$  value.

The LFRS story shear  $\mu_{FLx}$  depends on  $R_{DC}$  and the number of stories. The LFRS story

449 shear  $\mu_{FLx}$  decreases as the number of stories decreases. The LFRS story shear  $\mu_{FLx}$  decreases  
450 as  $R_{DC}$  increases. The LFRS story shear results  $\mu_{FLx}/\mu_{FL1-1}$  and  $\mu_{FLx}/\mu_{RE}$  are essentially  
451 independent of the number of stories. The LFRS story shear  $\mu_{FLx}/\mu_{FL1-1} \leq 1.0$  for  $R_{DC} \geq 1.5$ ,  
452 and  $\mu_{FLx}/\mu_{RE} \leq 0.8$  for every  $R_{DC}$  value.

453 The GLRS story shear  $\mu_{FLx}$  depends on the number of stories but it is not affected significantly  
454 by  $R_{DC}$ . The GLRS story shear results  $\mu_{FLx}/\mu_{FL1-1}$  and  $\mu_{FLx}/\mu_{RE}$  are similar and approximately  
455 equal to 1.0 for all  $R_{DC}$  and number of stories, with exception the four-story building which has  
456 GLRS story shear  $\mu_{FLx}/\mu_{RE} > 1.5$  for all  $R_{DC}$ .

457 The LFRS story drift  $\mu_{FLx}$  depends on  $R_{DC}$  and the number of stories. As  $R_{DC}$  increases the  
458 LFRS story drift  $\mu_{FLx}$  decrease. The effect of  $R_{DC}$  on the change of LFRS story drift  $\mu_{FLx}$  is  
459 more significant for the four-story building compared to the eight-story and twelve-story buildings.  
460 However, the LFRS story drift  $\mu_{FLx}$  remain less than 1.2% for all  $R_{DC}$  and number of stories. The  
461 LFRS story drift  $\mu_{FLx}/\mu_{FL1-1} \leq 1.0$  for  $R_{DC} \geq 1.7$  for all number of stories while it approaches a  
462 maximum value of 2.0 in the four-story building with  $R_{DC} = 0.8$ . All buildings have LFRS story  
463 drift  $\mu_{FLx}/\mu_{RE} \leq 1.0$ .

464 The GLRS story drift  $\mu_{FLx}$  in the eight-story and twelve-story buildings is similar and essentially  
465 independent of  $R_{DC}$ . The GLRS story drift  $\mu_{FLx}$  in the four-story building increases as  $R_{DC}$   
466 decreases and it is approximately equal to 2% for  $R_{DC} = 0.8$ . All buildings have  $\mu_{FLx}/\mu_{FL1-1} \leq$   
467 1.0. The twelve-story and eight-story buildings have GLRS story drift  $\mu_{FLx}/\mu_{RE} \approx 1.0$ . However,  
468 for the four-story buildings, as  $R_{DC}$  decreases the GLRS story drift  $\mu_{FLx}/\mu_{RE}$  increases.

### 469 **Variation of the twelve-story building periods of vibration under strong ground motion**

470 This section shows the effect of force-limiting deformable connections on the second mode  
471 seismic response of the twelve-story building. More specifically, this section compares the time  
472 variation of the periods of vibration of the building with RE connections with the time variation of  
473 the periods of vibration of the building with deformable connections designed for  $F_{Lx}$  with  $R_{DC} =$   
474 3.0, 2.0, and 0.8, during the first ten seconds of the ground motion EQ1 (listed in Table 4).

475 In general, the periods of vibration of a linear-elastic building model are determined from its

476 mass matrix and stiffness matrix. The nonlinear response of a building model changes the tangent  
477 stiffness during the response history while the mass remains constant. In this study, the first and  
478 second mode periods of vibration of the building models are calculated at the end of each converged  
479 time step of the nonlinear time history analysis from the constant mass matrix and tangent stiffness  
480 matrix.

481 Fig. 11(a) shows the first ten seconds of EQ1 ground acceleration time history. At approximately  
482 3.5 seconds, strong ground acceleration initiates and at approximately 7.0 seconds it ends. Fig.  
483 11(b) shows the pseudo-acceleration response spectrum of EQ1 in comparison with the ASCE/SEI  
484 7 design response spectrum. EQ1 has significantly larger spectral acceleration in the period region  
485 between 0.1 seconds and 0.5 seconds.

486 Fig. 11(c) through (e) show the time variation of the first mode period of vibration for the  
487 twelve-story building with RE connections and the time variation of the first mode period of  
488 vibration for building models with force-limiting deformable connections designed for  $F_{Lx}$  with  
489  $R_{DC} = 3.0, 2.0,$  and  $0.8,$  respectively, during the first ten seconds of EQ1. After the initiation of  
490 strong ground acceleration, the first mode periods of the buildings increase. As  $R_{DC}$  decreases the  
491 time variation of the first mode period in the buildings with force-limiting deformable connections  
492 approaches the variation of the first mode period in the building with RE connections. Deformable  
493 connections with smaller  $R_{DC}$  values have larger connection forces. The larger connection forces  
494 are transferred to the LFRS and develop larger LFRS story drift demand. The larger LFRS story  
495 drift demand results to leads to larger nonlinear rotation responses and reduced stiffness at the base  
496 flexural hinge of the LFRS (shear wall). As a result, the first mode period of vibration at the end of  
497 the strong ground motion acceleration approaches the first mode period of vibration of the building  
498 with RE connections.

499 Fig. 11(f) through (h) show the time that the second mode period of the building with  
500 RE connections is approximately constant while the second mode periods of the buildings with  
501 deformable connections are increased during the time of strong ground acceleration. As  $R_{DC}$   
502 decreases the variation of the second mode period is decreased.

503 Fig. 11(i) through (k) show the twelfth-floor total acceleration in the twelve-story building model  
504 with RE connections and twelfth-floor total acceleration in the building models with deformable  
505 connections. The deformable connections reduce the twelfth-floor total accelerations during and  
506 after the time of strong ground acceleration. At approximately 5.5 seconds of the time history,  
507 the twelfth-floor total acceleration of the building model with RE connections has large-amplitude  
508 response with an approximate period of 0.3 seconds which is close to the second mode period  
509 observed in Fig. 11(f) through (h); this result shows the importance of the second mode response  
510 to these large floor total accelerations. It is also noted that the twelve-story building model with  
511 deformable connections with smaller  $R_{DC}$  values have larger floor total accelerations during the  
512 time of the strong ground acceleration. Fig. 11(i) through (n) show the tenth-floor total acceleration  
513 in the building model with RE connections and the tenth-floor total acceleration in the building  
514 models with deformable connections. The tenth-floor is close to the node of the second mode shape  
515 of the building, and therefore, the tenth-floor total acceleration amplitude is significantly smaller  
516 than the twelfth-floor total acceleration amplitude in the building with RE connections. The tenth-  
517 floor total acceleration amplitude is similar to the twelfth-floor total acceleration amplitude in the  
518 building models with deformable connections.

519 These observations show that the force-limiting deformable connections modify the second  
520 mode seismic response of the twelve-story building while the nonlinear moment-rotation flexural  
521 base hinge response of the LFRS (shear wall) modifies primarily the first mode seismic response of  
522 the twelve-story building. The observations show that the effect of deformable connections on the  
523 seismic response of the building mitigates the contribution of the second mode to the total seismic  
524 response.

## 525 **Summary**

526 This paper presented (1) a force-based design method to determine the design value of the limiting  
527 force for the force-limiting deformable connection at each floor of buildings with LFRS that have

528 a base flexural mechanism (e.g., reinforced concrete shear wall buildings), (2) design examples,  
529 and (3) numerical simulations of twelve-story, eight-story, and four-story reinforced concrete shear  
530 wall example buildings with force-limiting deformable connections designed using the proposed  
531 method. The proposed design method is a modified version of the ASCE/SEI 7-16 (ASCE 2017)  
532 alternative seismic design force method for floor-diaphragms. The method is simple to implement  
533 in design practice. The method is also efficient since it does not require large number of parametric  
534 numerical earthquake simulations to determine feasible design space for the design values of the  
535 limiting force. The method provides design values for the limiting force that vary appropriately  
536 over the height of the building by considering the relative contributions of the first and higher  
537 modes to the seismic response of a building. The design examples showed the design values  
538 for the limiting forces of force-limiting deformable connections for twelve-story, eight-story, and  
539 four-story reinforced concrete shear wall example buildings. Seismic responses from numerical  
540 simulations of these example buildings with force-limiting deformable connections designed using  
541 the proposed design method were compared with the seismic responses of the example buildings  
542 with deformable connections with a constant limiting force over the height of the building, and with  
543 the seismic responses of the example buildings with RE connections, which represent conventional  
544 buildings. The effect of number of stories in the building and the magnitude of the limiting forces  
545 on the seismic response of the example buildings was studied. It was shown that the buildings with  
546 force-limiting deformable connections designed using the proposed method have a more uniform  
547 distribution of connection deformation demands over the height of the building compared to the  
548 buildings with deformable connections with a constant limiting force values over the height of the  
549 building. Larger design values of limiting force are required in the four-story building to have  
550 connection deformation demands similar to those of the eight-story and the twelve-story buildings.  
551 It was also shown that the buildings with force-limiting deformable connections designed using  
552 the proposed method have floor accelerations and force responses with reduced magnitude and  
553 dispersion compared to buildings with RE connections.

## Conclusions

- The proposed force-based method for design of force-limiting deformable connections enables simple and efficient calculation of the limiting force values required for preliminary design of these deformable connections that control the transfer of seismic-induced horizontal forces from the floor-diaphragms to the LFRS.
- Buildings with force-limiting deformable connections designed using the proposed method have reasonable connection deformation demands and relatively uniform distribution connection deformation demands over the height of the building.
- As the number of stories of the building decreases,  $F_{Lx}$  based on smaller  $R_{DC}$  value is required for reasonable connection deformation demands. It was observed that values of  $R_{DC}$  close to 1.5 for the twelve-story and the eight-story buildings and 1.0 for the four-story building result in acceptable seismic responses, even when a pin-based lean-on column model is assumed for the gravity load resisting system.
- The use of force-limiting deformable connections designed using the proposed method mitigates the contributions of the second mode response to the total seismic response of a building.

The proposed method is aimed at the preliminary design of force-limiting connections. Numerical simulations of the building with force-limiting deformable connections may be needed to assess the seismic response of the force-limiting connections, the LFRS, and the GLRS.

## Data Availability Statement

Some or all data, models, or code that support the findings of this study are available from the corresponding author upon reasonable request. Experimental data from previous research conducted for the development of the force-limiting deformable connections and the development of the friction devices referenced in this paper are available at DesignSafe-CI (Tsampras and Sause

578 2014a; Tsampras and Sause 2014b; Fleischman et al. 2014).

## 579 **Acknowledgments**

580 The authors are grateful for financial support provided by the Lehigh University and the Advanced  
581 Technology for Large Structural Systems (ATLSS) Engineering Research Center. Any opinions,  
582 findings, and conclusions expressed in this paper are those of the authors and do not necessarily  
583 reflect the views of others acknowledged here.

## 584 **REFERENCES**

- 585 ASCE, ed. (2010). *Minimum Design Loads for Buildings and Other Structures*. ASCE Standard.  
586 American Society of Civil Engineers : Structural Engineering Institute, Reston, Va.
- 587 ASCE (2017). *Minimum Design Loads*. ASCE, Reston, VA, seventh edition, [https://doi.org/10.](https://doi.org/10.1061/9780784414248)  
588 [1061/9780784414248](https://doi.org/10.1061/9780784414248).
- 589 Baker, J. W. (2011). “Conditional Mean Spectrum: Tool for Ground-Motion Selection.” *Jour-*  
590 *nal of Structural Engineering*, 137(3), 322–331, [https://doi.org/10.1061/\(ASCE\)ST.1943-541X.](https://doi.org/10.1061/(ASCE)ST.1943-541X.0000215)  
591 [0000215](https://doi.org/10.1061/(ASCE)ST.1943-541X.0000215).
- 592 Cao, L., Marullo, T., Al-Subaihawi, S., Kolay, C., Amer, A., Ricles, J., Sause, R., and Kusko,  
593 C. S. (2020). “NHERI Lehigh Experimental Facility With Large-Scale Multi-Directional Hybrid  
594 Simulation Testing Capabilities.” *Frontiers in Built Environment*, 6, 107, [https://doi.org/10.3389/](https://doi.org/10.3389/fbuil.2020.00107)  
595 [fbuil.2020.00107](https://doi.org/10.3389/fbuil.2020.00107).
- 596 Crane, S. T. (2004). “Influence of energy dissipation connections between floors and the lateral  
597 force resisting system.” *Report no.*, MS Thesis, UC San Diego, USA.
- 598 FEMA (2009). “Quantification of Building Seismic Performance Factors.” *Report No. FEMA*  
599 *P-695*, Federal Emergency Management Agency.
- 600 FEMA (2015). “NEHRP Recommended Seismic Provisions for New Buildings and Other Struc-  
601 tures.” *Report No. P-1050-1/2015*, Federal Emergency Management Agency.



602 FEMA (2017). “Guidelines for nonlinear structural analysis and design of buildings. part I -  
603 general.” *Report No. NIST GCR 17-917-46v1*, National Institute of Standards and Technology,  
604 Gaithersburg, MD, <https://doi.org/10.6028/NIST.GCR.17-917-46v1>.

605 Fleischman, R., Restrepo, J., Nema, A., Zhang, D., Shakya, U., Zhang, Z., Sause, R., Tsampras,  
606 G., and Monti, G. (2015). “Inertial Force-Limiting Anchorage System for Seismic Resistant  
607 Building Structures.” *Structures Congress*, Portland, Oregon, Structures Congress, 1302–1313,  
608 <https://doi.org/10.1061/9780784479117.111>.

609 Fleischman, R. B. and Farrow, K. T. (2001). “Dynamic behavior of perimeter lateral-system  
610 structures with flexible diaphragms.” *Earthquake Engineering & Structural Dynamics*, 30(5),  
611 745–763, <https://doi.org/10.1002/eqe.36>.

612 Fleischman, R. B., Restrepo, J. I., Sause, R., Zhang, D., Tsampras, G., Zhang, Z., Nema, A., and  
613 Shakya, U. (2014). “Half Scale Shake Table Test of a 4 Story Reinforced Concrete Building with  
614 Eccentric Shear Walls, <https://doi.org/10.4231/D39W0908G>.

615 McKenna, F. and Fenves, G. (2021). “The OpenSees Command Language Manual.

616 Moehle, J. P., Hooper, J. D., Kelly, D. J., and Meyer, T. R. (2010). “Seismic Design of Cast-in-  
617 Place Concrete Diaphragms, Chords, and Collectors.” *Report No. NIST GCR 10-917-4*, National  
618 Institute of Standards and Technology.

619 Ray-Chaudhuri, S. and Hutchinson, T. C. (2011). “Effect of Nonlinearity of Frame Buildings  
620 on Peak Horizontal Floor Acceleration.” *Journal of Earthquake Engineering*, 15(1), 124–142,  
621 <https://doi.org/10.1080/13632461003668046>.

622 Rodriguez, M. E., Restrepo, J. I., and Carr, A. J. (2002). “Earthquake-induced floor horizontal  
623 accelerations in buildings.” *Earthquake Engineering & Structural Dynamics*, 31(3), 693–718,  
624 <https://doi.org/10.1002/eqe.149>.

625 Sattar, S., McAllister, T., Johnson, K., Clavin, C., Segura, C., McCabe, S., Fung, J., Abrahams,  
626 L., Sylak-Glassman, E., Levitan, M., Harrison, K., and Harris, J. (2018). “Research needs to  
627 support immediate occupancy building performance objective following natural hazard events.”  
628 *Report No. NIST SP 1224*, National Institute of Standards and Technology, Gaithersburg, MD,

629 <https://doi.org/10.6028/NIST.SP.1224>.

630 Tsampras, G. (2016). “Force-Limiting Floor Diaphragm Connection for Earthquake-Resistant  
631 Buildings.” Ph.D. thesis, Lehigh University, USA, [https://preserve.lib.lehigh.edu/islandora/  
632 object/preserve%3Abp-10369972](https://preserve.lib.lehigh.edu/islandora/object/preserve%3Abp-10369972).

633 Tsampras, G. and Sause, R. (2014a). “Full-scale, components test of Inertial Force-Limiting Floor  
634 Anchorage Systems for Seismic Resistant Building Structures using a Buckling Restrained Brace  
635 and Steel Reinforced Low Damping Rubber Bearings, <https://doi.org/10.4231/D3N87311M>.

636 Tsampras, G. and Sause, R. (2014b). “Full-scale, components test of Inertial Force-Limiting Floor  
637 Anchorage Systems for Seismic Resistant Building Structures using a Friction Device and Carbon  
638 Fiber Reinforced Low Damping Rubber Bearings, <https://doi.org/10.4231/D3HH6C68B>.

639 Tsampras, G., Sause, R., Fleischman, R. B., and Restrepo, J. I. (2017). “Experimental study of  
640 deformable connection consisting of buckling-restrained brace and rubber bearings to connect  
641 floor system to lateral force resisting system.” *Earthquake Engineering & Structural Dynamics*,  
642 46(8), 1287–1305, <https://doi.org/10.1002/eqe.2856>.

643 Tsampras, G., Sause, R., Fleischman, R. B., and Restrepo, J. I. (2018). “Experimental study of  
644 deformable connection consisting of friction device and rubber bearings to connect floor system  
645 to lateral force resisting system.” *Earthquake Engineering & Structural Dynamics*, 47(4), 1032–  
646 1053, <https://doi.org/10.1002/eqe.3004>.

647 Tsampras, G., Sause, R., Zhang, D., Fleischman, R. B., Restrepo, J. I., Mar, D., and Maffei,  
648 J. (2016). “Development of deformable connection for earthquake-resistant buildings to reduce  
649 floor accelerations and force responses.” *Earthquake Engineering & Structural Dynamics*, 45(9),  
650 1473–1494, <https://doi.org/10.1002/eqe.2718>.

651 Van Den Einde, L., Conte, J. P., Restrepo, J. I., Bustamante, R., Halvorson, M., Hutchinson, T. C.,  
652 Lai, C.-T., Lotfizadeh, K., Luco, J. E., Morrison, M. L., Mosqueda, G., Nemeth, M., Ozelik, O.,  
653 Restrepo, S., Rodriguez, A., Shing, P. B., Thoen, B., and Tsampras, G. (2021). “NHERI@UC  
654 San Diego 6-DOF Large High-Performance Outdoor Shake Table Facility.” *Frontiers in Built  
655 Environment*, 6, 181, <https://doi.org/10.3389/fbuil.2020.580333>.

656 Zhang, D., Fleischman, R., Restrepo, J., Sause, R., Maffei, J., Mar, D., and Monti, G. (2014).  
657 “Development of a Floor Inertial Force Limiting Anchorage System Building Seismic Response.”  
658 *10th U.S. National Conference on Earthquake Engineering*, 10th U.S. National Conference on  
659 Earthquake Engineering, 11.

660 Zhang, Z., Fleischman, R. B., Restrepo, J. I., Guerrini, G., Nema, A., Zhang, D., Shakya, U.,  
661 Tsampras, G., and Sause, R. (2018). “Shake-table test performance of an inertial force-limiting  
662 floor anchorage system.” *Earthquake Engineering & Structural Dynamics*, 47(10), 1987–2011,  
663 <https://doi.org/10.1002/eqe.3047>.

664 **List of Tables**

665 1 Twelve-story building  $F_{Lx}$  for  $R_{DC} = 3.0$ . . . . . 29

666 2 Properties of the shear wall element. . . . . 30

667 3 Properties of the gravity column elements. . . . . 31

668 4 Eighteen ground motions selected from 44 FEMA P-695 far-field earthquake ground  
669 motion set. . . . . 32

670 5 Statistics of seismic responses for twelve-story buildings. . . . . 33

**TABLE 1.** Twelve-story building  $F_{Lx}$  for  $R_{DC} = 3.0$ .

Level $x$	$h_x/h_n$	$n_{Lx}$	$w_{px}/n_{Lx}$	$C_{Lx}$	$F_{Lx}$	$M_{F_{Lx}}$	$M_{bF_{Lx}}/M_{by}^a$
[-]	[-]	[-]	[kN]	[-]	[kN]	[MNm]	[-]
12	1.00	2	5916	0.77	1525	5	-
11	0.92	2	5916	0.62	1231	14	-
10	0.84	2	5916	0.48	937	26	-
9	0.76	2	5916	0.40	789	40	-
8	0.68	2	5916	0.40	789	57	-
7	0.60	2	5916	0.40	789	76	-
6	0.52	2	5916	0.40	789	98	-
5	0.44	2	5916	0.40	789	122	-
4	0.36	2	5916	0.40	789	149	-
3	0.28	2	5916	0.40	789	179	-
2	0.20	2	5916	0.40	789	211	-
1	0.12	2	5916	0.40	789	264	1.04

<sup>a</sup> $M_{by} = 253$  MNm

**TABLE 2.** Properties of the shear wall element.

Building	Beam-Column Elements			Base Hinge Spring Element	
	$A_w$	$I_{wcr}$	$E_c$	$M_{by} = \frac{M_{ELFI}}{\phi^a}$	$M_{bcap}$
[-]	[m <sup>2</sup> ]	[m <sup>4</sup> ]	[MPa]	[MNm]	[MNm]
12-Story	6.50	31.10	27800	253.0	569.0
8-Story	5.40	18.00	27800	154.0	384.0
4-Story	3.10	3.40	27800	58.0	145.0

<sup>a</sup> $\phi = 0.9$

**TABLE 3.** Properties of the gravity column elements.

Building	Stories	$E_c$	$A_c$	$I_c$
[-]	[-]	[MPa]	[m <sup>2</sup> ]	[m <sup>4</sup> ]
12-Story	1 <sup>st</sup> -6 <sup>th</sup>	27800	10.5700	0.4070
12-Story	7 <sup>th</sup> -12 <sup>th</sup>	27800	4.9960	0.0910
8-Story	1 <sup>st</sup> -4 <sup>th</sup>	27800	6.9780	0.2540
8-Story	5 <sup>th</sup> -8 <sup>th</sup>	27800	3.7260	0.0720
4-Story	1 <sup>st</sup> -4 <sup>th</sup>	27800	3.7260	0.0720

**TABLE 4.** Eighteen ground motions selected from 44 FEMA P-695 far-field earthquake ground motion set.

EQ [#]	Event [-]	Moment Magnitude [-]	Year [-]	Distance [km]	Soil Type Class [-]	Component [-]	PGA <sup>a</sup> [g]	PGV <sup>a</sup> [cm/sec]	SF <sup>b</sup> [-]
1	Friuli Italy	6.5	1976	15.0	C	TMZ000	0.35	22	2.77
2	Duzce Turkey	7.1	1999	12.0	D	BOL000	0.73	56	0.99
3	Superstition Hills	6.5	1987	11.2	D	B-POE270	0.45	36	1.87
4	Superstition Hills	6.5	1987	11.2	D	B-POE360	0.30	33	1.97
5	Chi-Chi Taiwan	7.6	1999	10.0	D	E-W	0.35	71	1.33
6	Chi-Chi Taiwan	7.6	1999	10.0	D	N-S	0.44	115	0.84
7	Landers	7.3	1992	19.7	D	CLW-LN	0.28	26	2.54
8	Imperial Valley	6.5	1979	22.0	D	H-DLT262	0.24	26	1.90
9	Imperial Valley	6.5	1979	22.0	D	H-DLT352	0.35	33	1.28
10	Imperial Valley	6.5	1979	12.5	D	H-E11230	0.38	42	2.06
11	Northridge	6.7	1994	9.4	D	MUL279	0.52	63	0.71
12	Superstition Hills	6.5	1987	18.2	D	ICC000	0.36	46	1.42
13	Loma Prieta	6.9	1989	12.2	D	G03090	0.37	45	1.40
14	Kocaeli Turkey	7.5	1999	13.6	D	DZC180	0.31	59	1.53
15	Kocaeli Turkey	7.5	1999	13.6	D	DZC270	0.36	46	0.93
16	Cape Mendocino	7.0	1992	7.9	D	RIO270	0.39	44	1.27
17	Kobe Japan	6.9	1995	19.1	D	SHI090	0.21	28	1.66
18	Landers	7.3	1992	23.6	D	YER270	0.24	51	1.24

<sup>a</sup>Peak ground acceleration (PGA) and peak ground velocity (PGV) for original earthquake ground motion records

<sup>b</sup>SF: Scale Factor to match design spectral accelerations over period range  $T \in [0.6, 2.0]$  seconds



**TABLE 5.** Statistics of seismic responses for twelve-story buildings.

Case	Floor		Connection				LFRS				GLRS			
	Total Acceleration		Force		Deformation		Shear <sup>a</sup>		Drift		Shear		Drift	
	$\mu$	$\frac{\sigma}{\mu}$	$\mu$	$\frac{\sigma}{\mu}$	$\mu$	$\frac{\sigma}{\mu}$	$\mu$	$\frac{\sigma}{\mu}$	$\mu$	$\frac{\sigma}{\mu}$	$\mu$	$\frac{\sigma}{\mu}$	$\mu$	$\frac{\sigma}{\mu}$
[-]	[g]	[-]	[kN]	[-]	[mm]	[-]	[kN]	[-]	[rad]	[-]	[kN]	[-]	[rad]	[-]
RE	1.52	50%	8986	50%	0	N/A <sup>b</sup>	33281	41%	0.013	21%	1704	18%	0.013	21%
F <sub>L1-1</sub>	0.65	19%	2532	10%	121	26%	17026	10%	0.010	18%	1558	26%	0.019	18%
F <sub>L1-2</sub>	0.67	18%	2466	11%	163	22%	15077	9%	0.008	17%	1562	25%	0.020	18%
R <sub>DC</sub> = 0.8	0.99	6%	5699	5%	14	70%	23927	10%	0.012	20%	1627	19%	0.013	17%
R <sub>DC</sub> = 1.0	0.82	5%	4641	2%	17	64%	22265	9%	0.012	20%	1664	19%	0.013	18%
R <sub>DC</sub> = 1.5	0.63	20%	3201	2%	28	39%	18887	8%	0.011	20%	1615	20%	0.012	20%
R <sub>DC</sub> = 2.0	0.60	25%	2632	5%	54	31%	16737	9%	0.010	17%	1589	22%	0.013	24%
R <sub>DC</sub> = 2.5	0.61	23%	2383	7%	77	24%	15167	12%	0.009	17%	1561	20%	0.013	20%
R <sub>DC</sub> = 3.0	0.61	23%	2198	9%	91	25%	14524	11%	0.008	19%	1597	21%	0.012	17%

<sup>a</sup>Design base shear from ASCE/SEI 7 equivalent lateral force procedure is 7835 kN.

$\mu$  is the mean value of the maximum peak floor or story responses over the set of ground motions.

$\sigma$  is the standard deviation value of the maximum peak floor or story responses over the set of ground motions.

$\frac{\sigma}{\mu}$  is the coefficient of variation.

<sup>b</sup>The deformation of rigid connection does not vary and it is essentially zero.

# List of Figures

671

672 1 Schematic overview of building with planar shear walls and force-limiting de-

673 formable connections and schematic of friction device (Tsampras et al. 2018). . . . . 35

674 2 Design acceleration coefficient variation for buildings with (a) 2 or less floors and

675 (b) 3 or more floors. . . . . 36

676 3 Path of seismic-induced horizontal forces. . . . . 37

677 4 (a)  $C_{Lx}$  acceleration coefficient. (b) Deformable connection design forces  $F_{Lx}$ . (c)

678 LFRS free body diagram subjected to connection design forces  $F_{Lx}$ . . . . . 38

679 5 (a) Typical example building floor plan. (b) Schematic of typical example building

680 numerical model. (c) Typical deformable connection force-deformation response.

681 (d) Typical LFRS base hinge moment-rotation response. . . . . 39

682 6 Limiting force values for four-story, eight-story, and twelve-story buildings. . . . . 40

683 7 Pseudo acceleration response spectra for 18 ground motions, median pseudo accel-

684 eration spectrum, and design response spectrum for 5% damping. . . . . 41

685 8 Seismic response results for twelve-story buildings. . . . . 42

686 9 Seismic response results for eight-story and four-story buildings. . . . . 43

687 10 Variation of  $\mu_{FLx}$  (Row 1),  $\mu_{FLx}/\mu_{FL1-1}$  (Row 2), and  $\mu_{FLx}/\mu_{RE}$  (Row 3) with

688 respect to  $R_{DC}$  value and number of building stories. . . . . 44

689 11 (a) Earthquake ground acceleration time history (EQ1). (b) EQ1 response spectrum

690 and ASCE/SEI 7 design response spectrum for 5% damping ratio. (c) through (h)

691 First mode and second mode periods for twelve-story building models with RE

692 connections and deformable connections designed for  $F_{Lx}$  with  $R_{DC} = 3.0, 2.0, 0.8$

693 subjected to EQ1. (i) through (n) twelfth-floor and tenth-floor total acceleration time

694 histories of twelve-story building models with RE connections and with deformable

695 connections designed for  $F_{Lx}$  with  $R_{DC} = 3.0, 2.0, 0.8$  subjected to EQ1. . . . . 45

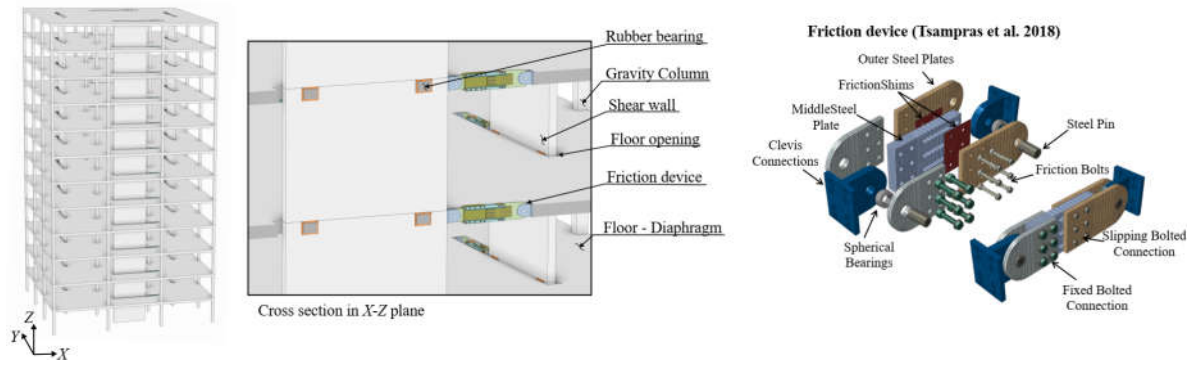


**Fig. 1.** Schematic overview of building with planar shear walls and force-limiting deformable connections and schematic of friction device (Tsampras et al. 2018).

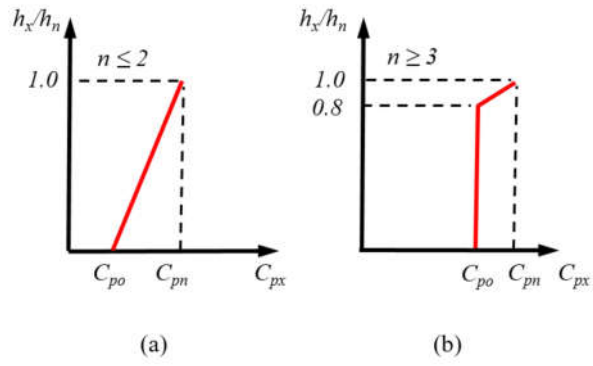


**Fig. 2.** Design acceleration coefficient variation for buildings with (a) 2 or less floors and (b) 3 or more floors.

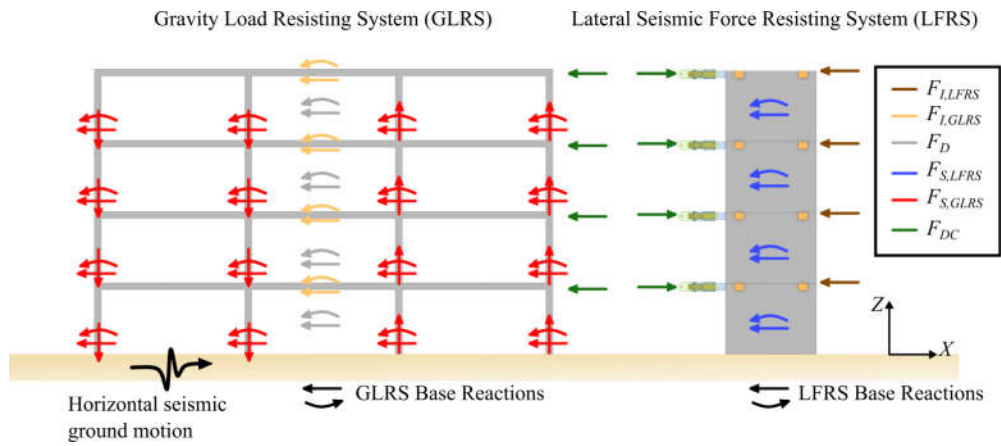


**Fig. 3.** Path of seismic-induced horizontal forces.

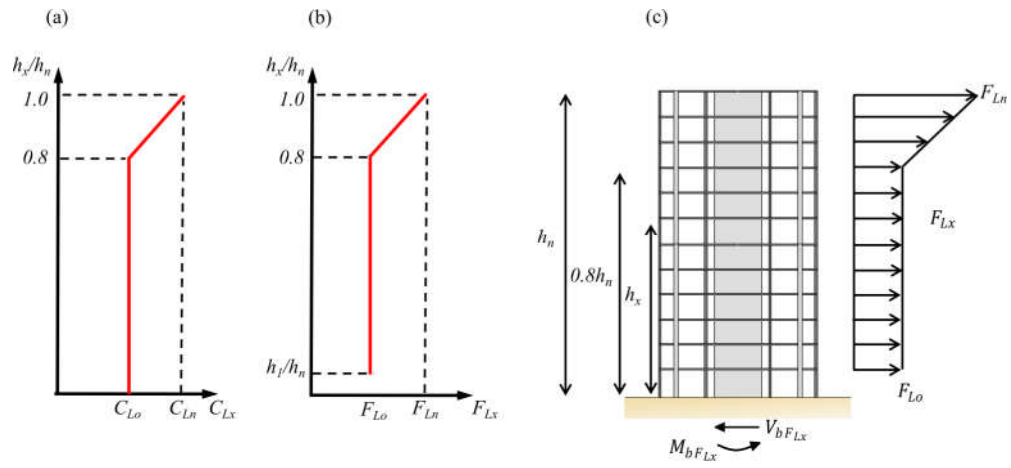


**Fig. 4.** (a)  $C_{Lx}$  acceleration coefficient. (b) Deformable connection design forces  $F_{Lx}$ . (c) LFRS free body diagram subjected to connection design forces  $F_{Lx}$ .

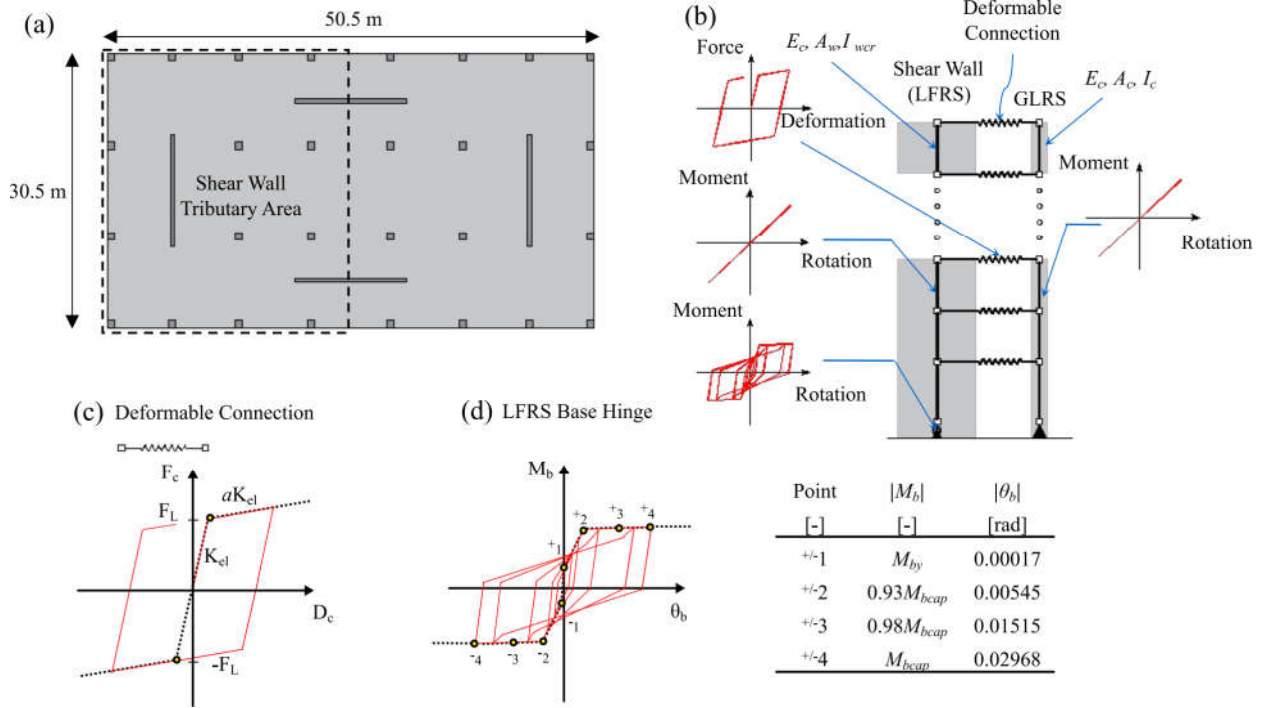


**Fig. 5.** (a) Typical example building floor plan. (b) Schematic of typical example building numerical model. (c) Typical deformable connection force-deformation response. (d) Typical LFRS base hinge moment-rotation response.

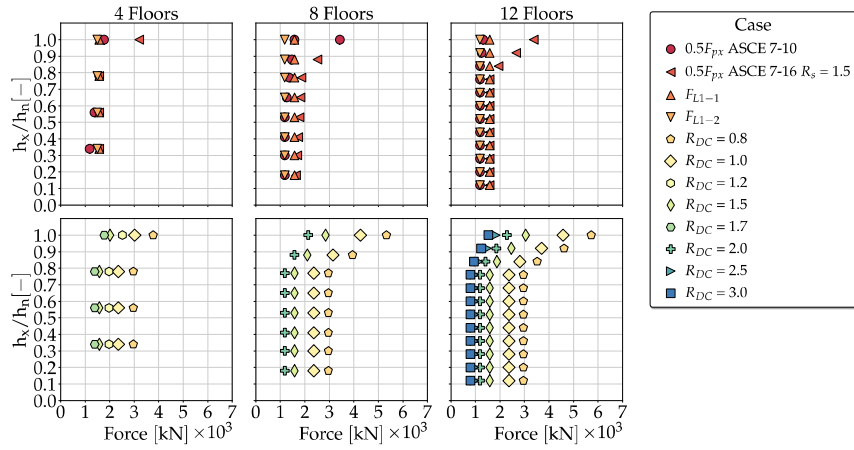


**Fig. 6.** Limiting force values for four-story, eight-story, and twelve-story buildings.



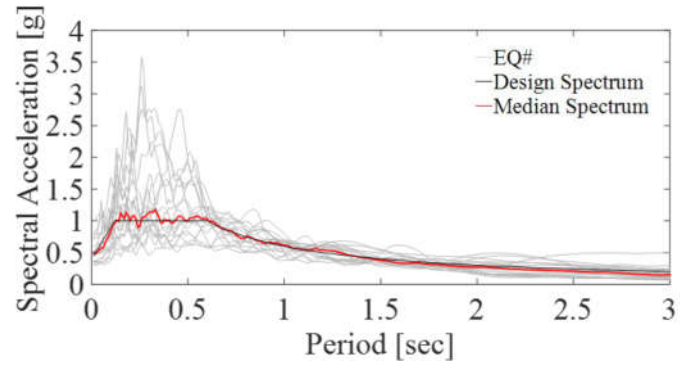


**Fig. 7.** Pseudo acceleration response spectra for 18 ground motions, median pseudo acceleration spectrum, and design response spectrum for 5% damping.

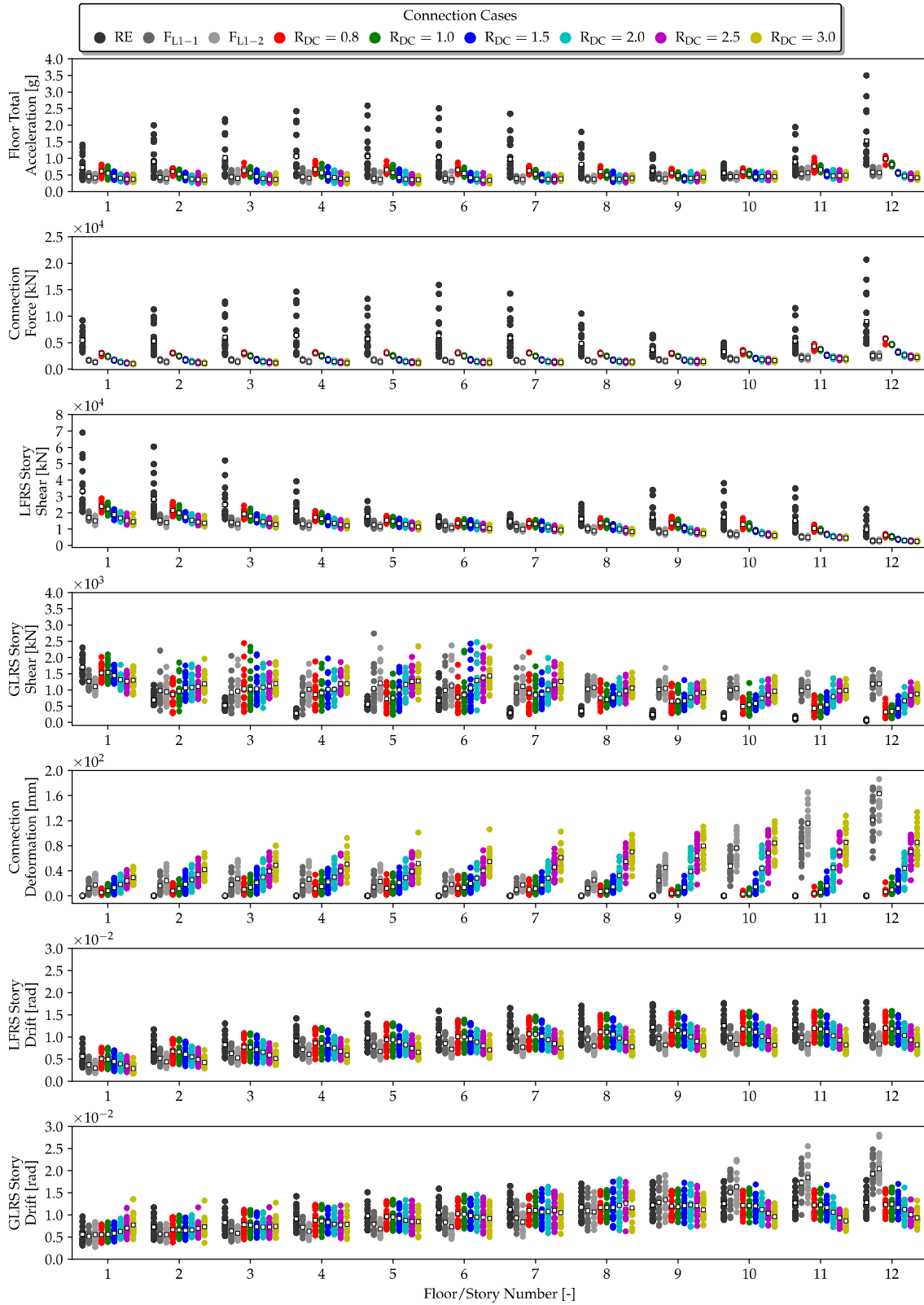


**Fig. 8.** Seismic response results for twelve-story buildings.

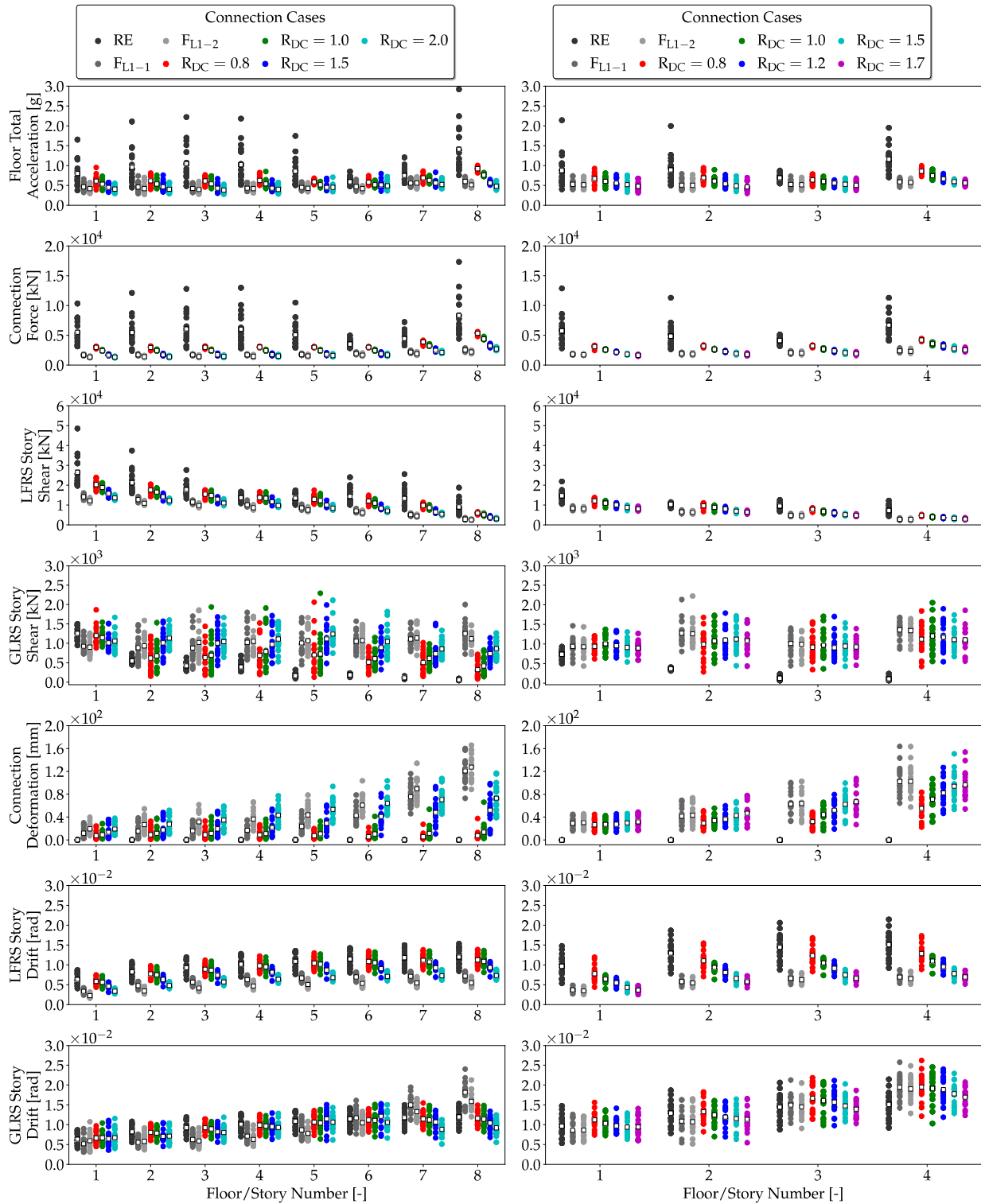


**Fig. 9.** Seismic response results for eight-story and four-story buildings.

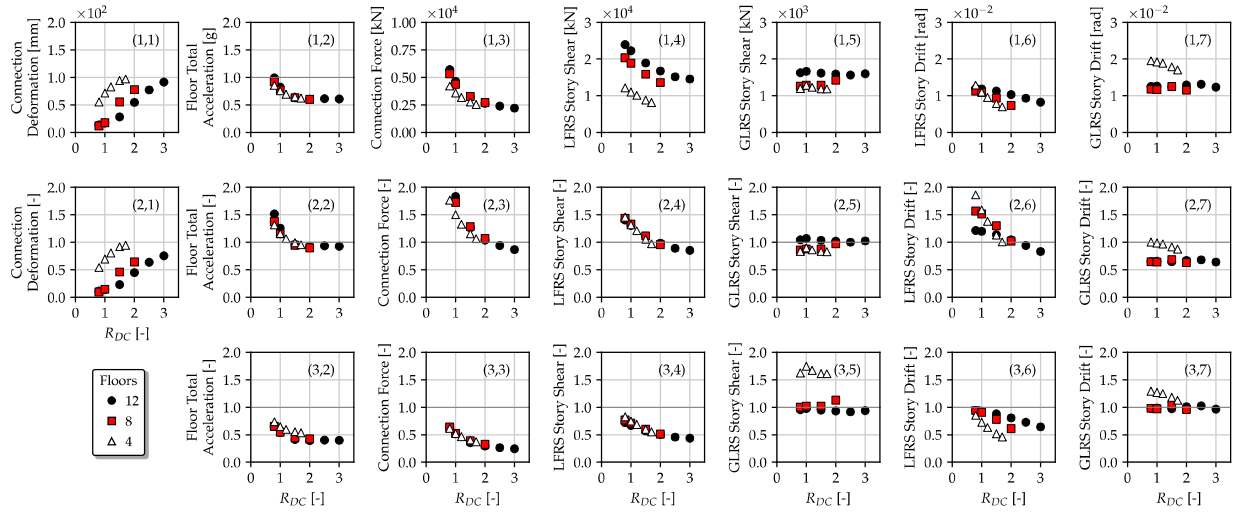


**Fig. 10.** Variation of  $\mu_{FLx}$  (Row 1),  $\mu_{FLx}/\mu_{FL1-1}$  (Row 2), and  $\mu_{FLx}/\mu_{RE}$  (Row 3) with respect to  $R_{DC}$  value and number of building stories.

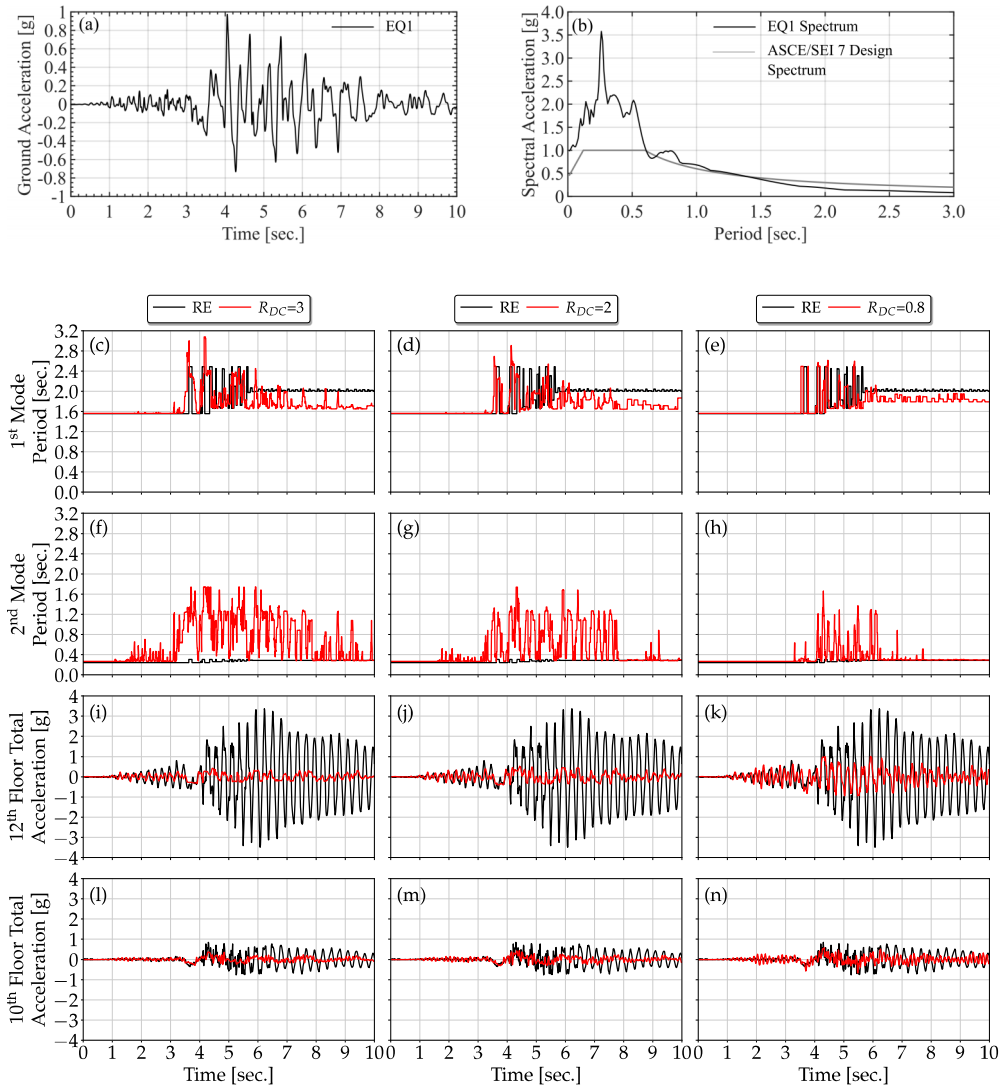


**Fig. 11.** (a) Earthquake ground acceleration time history (EQ1). (b) EQ1 response spectrum and ASCE/SEI 7 design response spectrum for 5% damping ratio. (c) through (h) First mode and second mode periods for twelve-story building models with RE connections and deformable connections designed for  $F_{Lx}$  with  $R_{DC} = 3.0, 2.0, 0.8$  subjected to EQ1. (i) through (n) twelfth-floor and tenth-floor total acceleration time histories of twelve-story building models with RE connections and with deformable connections designed for  $F_{Lx}$  with  $R_{DC} = 3.0, 2.0, 0.8$  subjected to EQ1.